Simulation of resistance forces acting on surgical needles

5 authors, including:

Alison S Carr
Qatar University
57 PUBLICATIONS   **811** CITATIONS

SEE PROFILE

Some of the authors of this publication are also working on these related projects:

Clinical problem solving and situational judgement tests for selection View project

Selection into Specialty Training View project

Simulation of resistance forces acting on surgical needles

P N Brett[1], **T J Parker**[1], **A J Harrison**[1], **T A Thomas**[2] and **A Carr**[2]
[1] AMARC, Department of Mechanical Engineering, University of Bristol
[2] Department of Anaesthesia, University of Bristol

Abstract: High precision in the manual control of needles and biopsy probes in medical treatment requires high skill and dexterity levels. In anaesthesia, force sensation is an important feedback mechanism, and the practitioner needs to refresh or develop skills to improve on the interpretation of needle progress towards the target site. This paper describes an experimental tactile force simulator for uniaxial needle action for which the force resisting progress of the needle is derived from measured data. As an example, the approach taken to develop the simulation of the insertion of epidural needles is described. Adaptation to other procedures would be possible by adopting new reference models based on appropriate measured force data.

Keywords: soft tissues, needles, epidural, simulation

NOTATION

A	surface area of needle in contact with tissues
$\{a_0, \ldots, a_n\}$, $\{b_1, \ldots, b_2\}$	constant coefficients
F	force
$H(x)$	Heavisides' function
k, k_0	elastic moduli
n	index of incremental time step
N	total number of time steps
R_a	radius of needle
V	velocity
V_d	velocity demand
x	displacement
x_{max}	maximum displacement before rupture
α, β	non-linear elastic coefficients
Δt	incremental time step
η	viscosity

1 INTRODUCTION

The skill levels required of practising surgeons and anaesthetists is likely to increase, particularly in procedures performed through small incisions, such as in minimal access therapy, the application of anaesthetic blocks and the insertion of biopsy needles to targets deep within the body. To achieve high levels of precision requires the acquisition of both visual and tactile sensations, which give the potential to improve tool control.

Research studies have recently demonstrated the potential benefits that automation technology can contribute to invasive treatment, working both in rigid tissues (**1, 2**) and more recently in soft tissues (**3, 4**). When working with soft tissues, devices have been demonstrated that take the tissue deformation into consideration in order to achieve high positional accuracy. In such applications automation technology has demonstrated the potential to enhance skills through the development of new tools.

Automation technology can also be applied to improve skills through simulation. Visual simulation is a subject of current research (**5, 6**); however, the sense of touch is also important and there are procedures where tool control relies heavily on touch sense. One such set of procedures involves the precise positioning of needles to deliver anaesthetic fluid locally in the body. An increased availability of suitable methods for improving skills through training would reduce risks to patients (**7**).

To insert a needle first requires the identification of the insertion point and trajectory based on an assessment of the target position from surface features, palpation and possibly scan data, together with a knowledge of the underlying anatomy. Progress of the needle in the body can be judged from the proportion of the needle

remaining outside and the tactile force experienced during injection. An experienced practitioner is able to interpret the position of the needle relative to the tissue type more accurately than a practitioner developing new skills and it is unfortunate that in most cases this experience can only be achieved by *in vivo* practice (on patients). Public opinion and laws preventing cruelty to animals exclude the use of living animals for training, and cadaver specimens are not always representative or available. Therefore, artificial physical models based on a composite of materials have been used to provide the appropriate tactile experience (**8**); however, these are not always reliable or consistent and certainly cannot provide feedback to the trainee on how their skill compares with that of an experienced user or standard. There is also a need to represent different patient types (obesity, age, fitness), and to provide conditions from which the sensation resulting from an error in trajectory or motion can be experienced. A simulator that provides this experience will be useful in improving treatment.

This paper describes the method adopted in the development of a tactile computer simulation training device for linear axis needle action as would be appropriate for administering injections in soft tissues. The paper focuses on the implementation of the machine to simulate the epidural anaesthetic procedure by providing the sensation of needle velocity response to the force applied. In the epidural procedure a Tuohy needle is advanced from the surface of the body to the epidural space and penetrates a variety of tissue types along the trajectory. The change in needle velocity response to applied force provides the anaesthetic with the indication of progress through tissue layers. Finally the progress of the needle through a tough ligament into the cavity of the epidural space must be controlled. The simulator also makes provision for the loss in resistance of fluid compressed in the syringe as part of a well-used technique to detect entry of the needle into the epidural space.

The approach adopted is described in the following sections. Needle force was measured by inserting Tuohy needles in appropriate tissue structures to simulate the epidural with the intention to find the relationship between needle velocity response to applied force. The response is dependent on time, needle displacement, the instantaneous needle velocity and on the tissues penetrated. In practice the velocity response will vary between cases as tissue thicknesses and state are not consistent between patients. Results from a programme of experimental measurements of needle force with respect to velocity revealed three prominent features of force, and corresponding needle velocity response. Analysis of the measurements has shown that these features can be represented by simple mathematical functions that can be used to determine the needle velocity demand signal to the simulator controller with respect to the force applied, needle insertion depth, tissue type and thickness. Simulations of needle velocity response by use of these
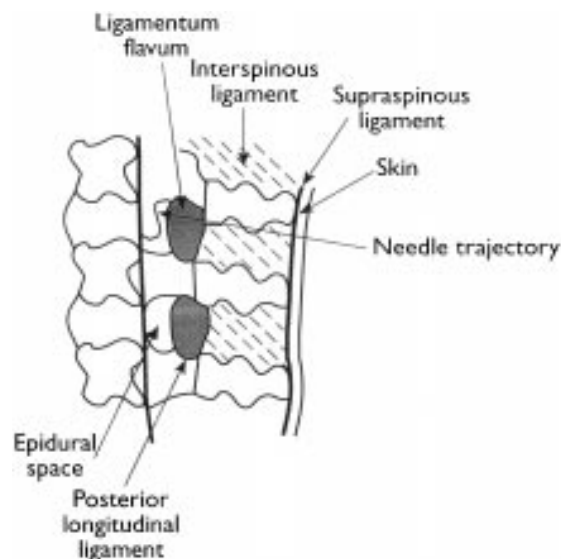

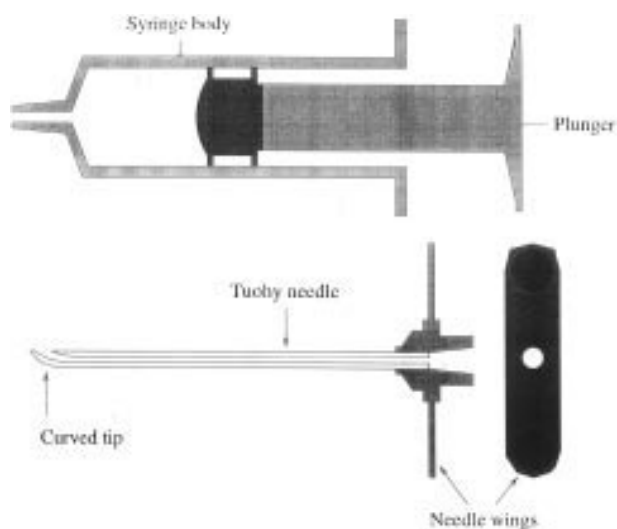**Fig. 1a** Tissue layers in an epidural procedure

Fig. 1b Diagram of the hollow Tuohy needle and syringe

functions and the superimposed frictional functions have then demonstrated reasonable representation of the force and velocity response at the prominent stages that are used to interpret needle progress by some anaesthetists.

The approach adopted has used a simple actuating mechanism involving only single linear axis of movement of the needle as opposed to a universal system of complex geometry (**9**). Such a system could eventually be produced cost effectively to suit small groups of anaesthetists.

This paper first describes the epidural procedure at the focus of the investigation, and provides a description of the simulator system and component parts. The description of the forces and velocity response encoun-

tered in different tissue layers leads on to the approach used to represent this behaviour. Finally, the performance and force sensation experienced are described.

2 THE EPIDURAL PUNCTURE

An epidural is the procedure that places anaesthetic locally in the epidural space within the spinal canal surrounding the spinal cord. The layers of tissue penetrated by the needle are skin and fatty tissue, followed by the supraspinous ligament, intraspinous ligament and finally the tough ligamentum flavum as shown in Fig. 1a. The media represent membrane structures, fatty tissue, ligament tissues and the ligament–cavity interface. The procedure is used extensively in labour, obstetrics and for other forms of anaesthesia. A Tuohy needle and syringe are used and these are shown in Fig. 1b. To carry out the procedure the tip of the hollow Tuohy needle is inserted into the epidural space within the spinal canal. The needle must be accurately positioned in the epidural space to allow insertion of a catheter or injection of local anaesthetic into the epidural space. To achieve accurate placement and avoid complications requires rapid reaction to the change in resistance on advancing the needle.

The epidural space is small and to enter requires penetration of a tough ligament. Overshoot of the needle across the epidural space must be minimized to avoid penetration of the dura surrounding the spinal cord, and complications and considerable discomfort for the patient. The level of overshoot is dependent on the method of gripping and supporting the needle as well as the stance adopted by the anaesthetist. A simulation of needle response will provide the potential to improve skills with respect to response at this crucial stage in the procedure.

During the administration of an epidural, the patient is usually in a sitting position and leaning forward to enlarge the available space for the needle to be inserted between the vertebrae. Tool force is an essential navigation aid to the epidural procedure. Confirmation that the Tuohy needle has entered the epidural space is based on a sign called loss of resistance. The sign depends on the application of pressure to the contents, air or normal saline, of a syringe attached to the Tuohy needle. The pressure would normally inject fluid through the needle. However, while the needle tip is within dense ligaments, injection of fluid is not possible. When the tip suddenly enters the epidural space resistance to injection disappears and tip placement in the epidural space is confirmed.

If most of the force driving the Tuohy needle through ligaments has been applied via the syringe plunger, entry of the needle tip into the epidural space will not only lose resistance to injection but will also remove the force driving the Tuohy forwards.

3 THE SIMULATOR SYSTEM

A schematic diagram of the simulator system is shown in Fig. 2. The applied tool force is measured using a strain-gauged sensor, and by using the position and velocity measurements, provides the input to the motion function that describes the resulting needle response in tissues. The model types used to represent needle velocity response to the force applied are based on the Voigt spring-dashpot configurations (10) with different values for coefficients of springs and dashpots appropriate to needle progress through the tissue layers as experienced during measurements. To accommodate different techniques, the simulator system has been constructed to provide both the tool force sensation and the loss of resistance to injection of air or saline fluid within the syringe by triggering an electrofluid valve to enable discharge of pressurized fluid from the syringe.

The motion function outputs a velocity demand to the velocity servo system. The controller used is a commercial, hardwired, proportional + integral + derivative (PID) type, driving a carriage against a force sensor using a direct current (DC) motor and ball screw. The construction is shown in Fig. 3.

The response of the system needs to be such as to provide the correct sensation. It is known that the human tactile system comprises the combined response of a variety of types of nerve terminals in skin tissue (11). These convey information for different types of receptors providing a range of sensitivities to important surface actions such as indentation, contact and slip. There is variation between response of receptor types and the transmission of signals. This leads to a variation in sensitivity to contact forces depending on how objects, such as Tuohy needles, are held. During the epidural procedure, the practitioner monitors changes in force level associated with the peaks in force. The method of gripping and guiding the needle and syringe is adapted to maximize sensitivity despite wearing surgical gloves. In devising the simulator it has been important to ensure that the response of controller and mechanism is sufficiently fast to avoid perceptible deviation from the demand signal. Selection of a high bandwidth achieves this by avoiding resonance. The lower limit to bandwidth is mechanical response, while the higher limit is governed either by the need to avoid sensitivity to noise as a result of a high sampling rate, or the electronic limitations of the data acquisition hardware. Based on empirical evidence of apparent acceptability, a system bandwidth of 100 Hz was used. As expected, the limiting condition is the representation of penetration through the ligamentum flavum where there is an abrupt change in the required response. This performance is in agreement
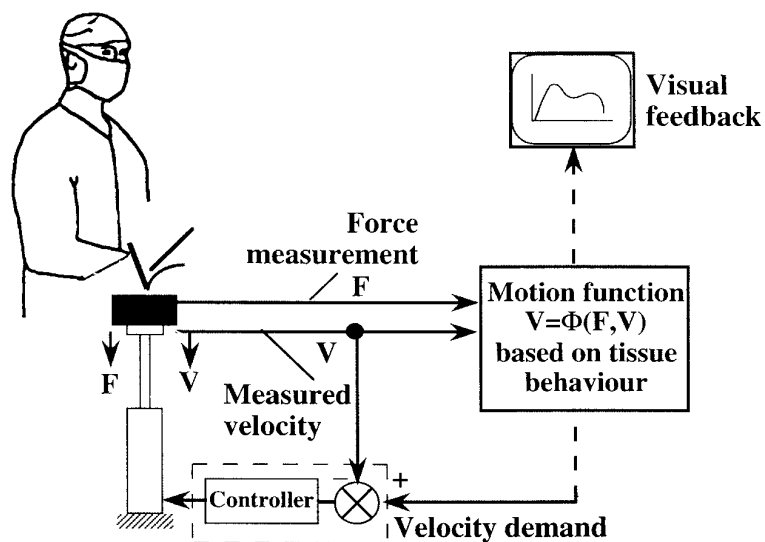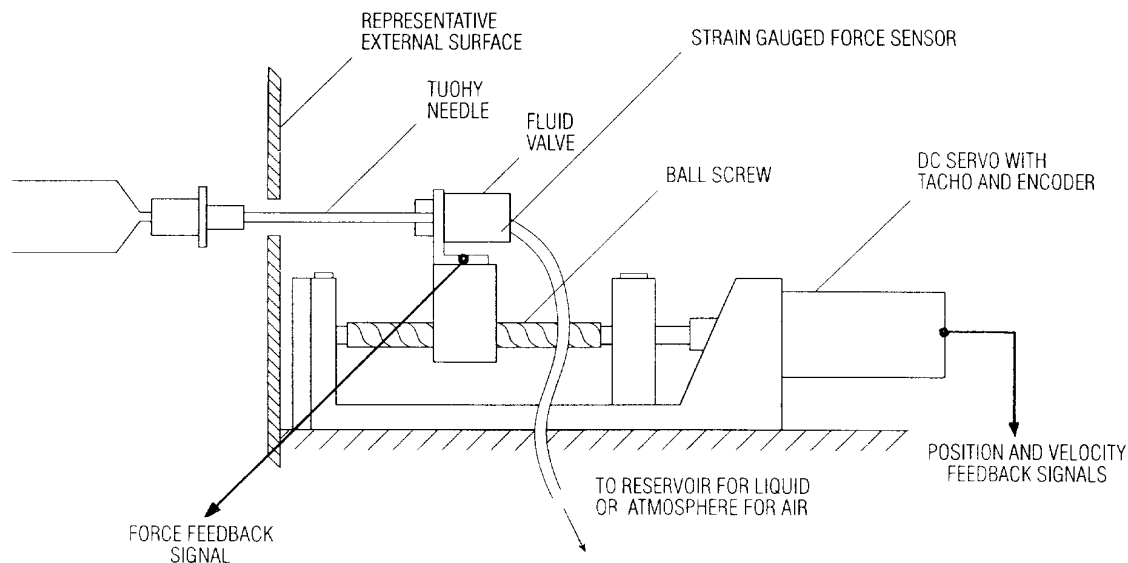
Fig. 2   Schematic diagram of the simulator system

Fig. 3   Diagram showing the mechanical construction of the simulator

with broad estimates of human response determined by others (**12**).

4   FORCE MEASUREMENTS

Measurements of the force response of a Tuohy needle moving at constant velocity while penetrating tissues have been made to identify the character of the principal features in the force response. This was accomplished using an instrumented syringe and needle that was advanced into porcine samples in a tensile test machine, and cadavers by hand. Ideally, it may be considered that measurements need to be retrieved from live patients.

However, needle force is dependent on needle velocity which will vary under manual application. Under such inconsistent input it is difficult to retrieve the fundamental relationship between force and tool response in this case. Hand-held measurements on the recently deceased provided verification of force levels and transients obtained from porcine specimens.

The needle and syringe are of the same form as conventional types, and these have been adapted with sensors such as to avoid contact with the patient. Originally devised for use on live patients, the set-up can be made sterile and avoids any interference with the procedure. However, the success of the approach for determining force sensation using fixed cadavers, porcine samples and

recently deceased cadaver specimens has led to trials on patients being postponed.

Fixed cadavers have provided information on tissue separation and thickness. The advantages of using fixed cadaver specimens are the availability and appropriate size and form. However, the cool temperature of tissues, the past effects of rigour and the introduction of formaldehyde have a significant effect on the toughness and deformation properties of soft tissues. As a result, force levels for puncturing membranes and ligament tissues are higher than expected in a live patient (**13**). The tests have led to techniques for measurements on recently deceased cadavers.

Laboratory tests on porcine samples were performed (2–5 hours after death). Accurate feed of needles into the epidural space of samples was achieved in a tensile test machine. These measurements have enabled an accurate determination of needle force transients corresponding with constant needle velocities and a knowledge of the tissue types and thicknesses encountered. Using a feed rate of 60 mm/min the typical force response is shown in Fig. 4a. These data show the three primary peaks corresponding with important tissue interfaces. In region 1 the peak force corresponding with needle penetration of the supraspinous ligament can be seen clearly. Region 2 represents the needle penetrating through muscle fibre. The force peak of 15 N in region 3 is experienced as the needle penetrates the ligamentum flavum.

By measuring force response at different constant needle velocities the relationship between changes in the features such as peak force values to changes in velocity could be determined. A typical variation in the liga-
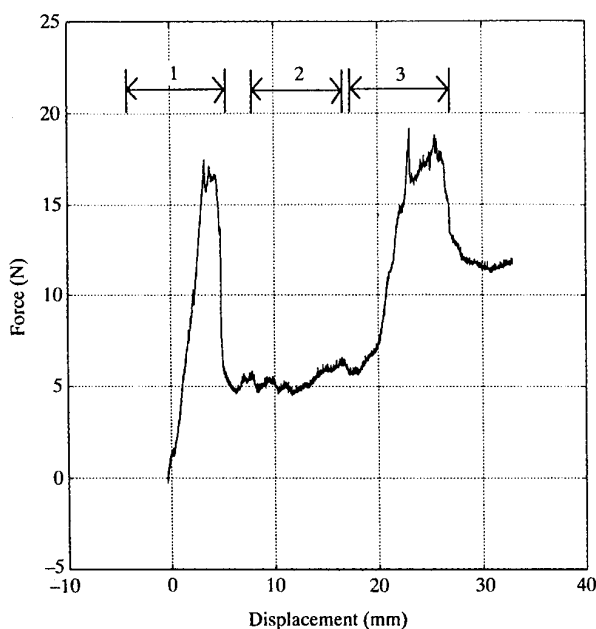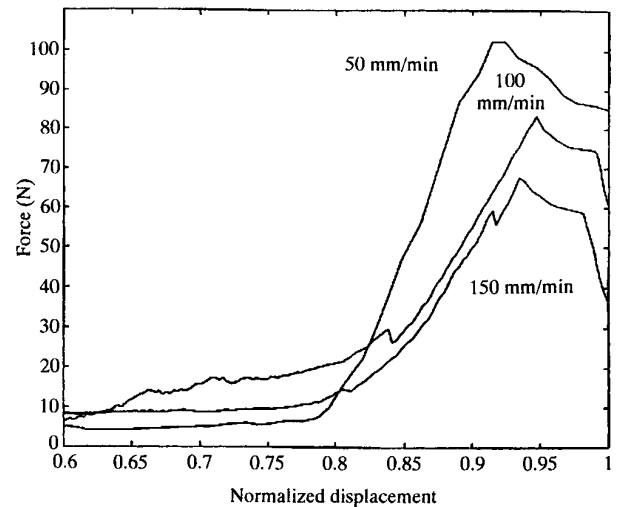

Fig. 4b Typical variation in the ligamentum flavum peak force curves for different needle velocities

mentum flavum peak force curves for different needle velocities is shown in Fig. 4b. It can be seen that the overall force profile of the feature does not change, whereas the peak value does. Puncture forces in membranes are reduced at higher needle velocities as the underlying tissues deflect with time dependent behaviour and this prevents significant deflection of the membrane before puncture occurs. During implementation of the simulator, demand signals to the controller of the mechanism need to reflect the velocity dependence while providing a consistent profile of the feature.

During trials in the mortuary on the recently deceased, force was derived from syringe fluid pressure. This approach is similar to that used by Holloway and Telford (**14**). The needle is advanced into the body by pushing on the end of the syringe rather than directly on the Tuohy needle part of the assembly. During insertion, as the saline fluid is trapped within the syringe and needle, the stiffness between the plunger and needle is much higher than the stiffness of the deflecting tissues. Measurement of pressure gives a reliable means of determining force, and this was confirmed in the laboratory by using a tensile test machine. Example force versus pressure calibration curves are shown in Appendix 1. The pressure is measured using a transducer at the termination of a short line configured at the infusion tapping port. Before insertion, care was taken to expel any air bubbles in the system. A deviation between the needle force and the force indicated by syringe pressure occurs with motion of the plunger in the syringe, such as when fluid is expelled into the cavity of the dural space. Under these conditions the indicated force is higher than the true force by approximately 1 N and is due primarily to friction. To measure displacement, a scheme using the reflectance intensity from a light-emitting diode (LED) emitter/detector pair

Fig. 4a Typical force response at a feed rate of 60 mm/min

mounted on the syringe was used. The experimental arrangement is shown in Fig. 5a. To avoid the effect of ambient light, a technique was developed to subtract the ambient component by switching the emitter at every sample period and detecting the corresponding change

in intensity. The transducer signal and photo-transistor voltage were sampled using a commercial analogue-to-digital converter attached to a portable computer. The calibration for reflectance was carried out during the trials as the surface of the cadaver had an influence on
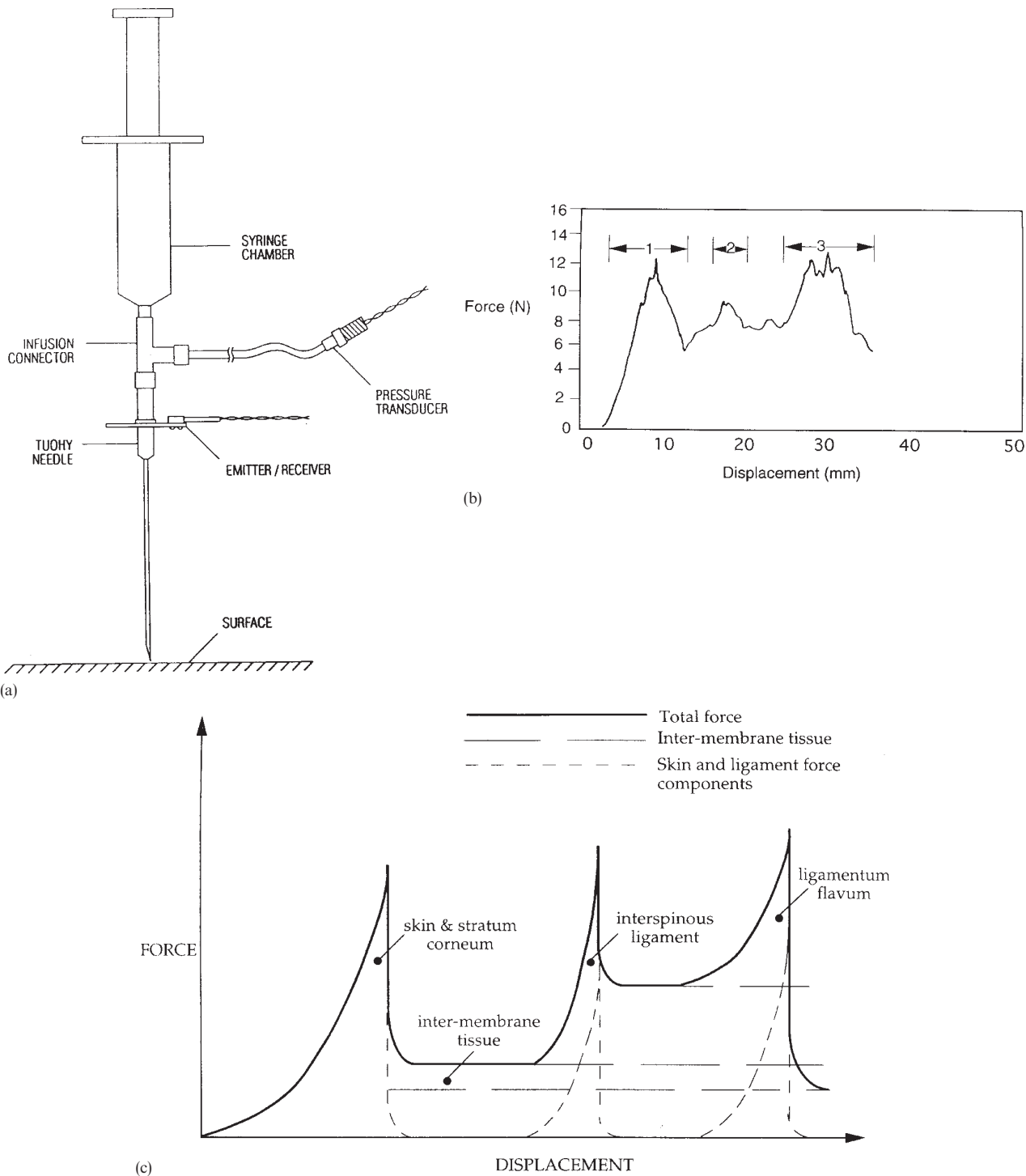

Fig. 5   (a) Experimental set-up; (b) typical force transients obtained; and (c) schematic superposition of force components

reflective values. The calibration curve is non-linear and is easily interpreted using the connected personal computer (PC). Pre-trial calibration curves are shown in Appendix 2. Typical force transients obtained when using this equipment are shown in Fig. 5b. The peaks in force are to be found corresponding with the same tissue types as found in the studies on porcine samples mentioned above. The shape of the force peaks are also similar to the porcine data and this suggests that the form of models developed from porcine data will correlate with human specimens. Deviations between the data sets are primarily due to the extremely high bursting strength and elasticity of porcine skin, which affects the initial rupture force peak and subsequent frictional forces due to tissue clamping of the needle. This last effect shows a marked dependence on the degree of hydration of the sample, with lower levels of hydration leading to higher measured force levels.

From the measured data it is observed that the force characteristics take the form of a combination of stepped, increasing friction levels corresponding with sliding through additional tissues. The dominant effects are due to the clamping forces of the penetrated tissue and are illustrated in Fig. 5c. Superimposed on the stepped frictional component are puncture force transients showing non-linear elastic behaviour with subsequent time dependent recovery of membrane and tissues following puncture. Other effects, such as increasing shear force with needle depth are much less significant. To provide a representative sensation of these effects a simulator requires mathematical representation of the data corresponding with these principal elements. The order in which tissue layers are encountered is known; however, the timing of peaks is unknown and is dependent on needle feed and on the separation between tissues and tissue thickness. The characteristics are known to vary between cases and are dependent on sex, age and build. It should be noted that while the general form of the force transients was consistent between cases, the value of peak forces varied by as much as 90 per cent. It is anticipated that further trials on a wide range of samples will reveal typical values for model representation of these differences. To illustrate a method for simulation, model representations are based on the typical experimental results of Fig. 4a.

5 MODELS OF TOOL FORCE AND RESPONSE

During passage of the needle through the various tissues there are a combination of processes taking place from cutting, sliding, stick–slip, tissue deformation and displacement and peeling. To aid in the characterization of the velocity response of the needle in the different layers and to simplify the modelling process, simple models demonstrating the observed overall behaviour of actual tissues were used. These may be viewed as similarity

relationships between the model and the tissue which exhibit the same type of response.

The velocity response of needles penetrating soft tissues can be described as principally elastic, viscous or viscoelastic. For example the mechanical properties of adipose tissue have been shown empirically to be almost completely viscous with a force opposing motion very nearly proportional to the speed of insertion and the area of tool exposed. In contrast, the properties of muscle fascia are strongly elastic. In building a representative model of the expected force profiles during a complete procedure, the individual tissues have been modelled using simple combinations of viscous and elastic elements and the Voigt model has been used as the basis for the modelling element (15) in this approach. It is noted that other forms of element could have been used including polynomial laws (16). The element types were chosen for their ease of manipulation to obtain an adequate match with the observed tissue behaviour. The order in which the tissue layers are encountered is known and indeed for the simulation the initial separation and thickness is defined. Models to describe the influence of newly encountered tissue on needle velocity response, in addition to the effect of preceding tissues, can be combined in the appropriate order. The responses produced by muscle, skin and ligamental tissue are dominated by elastic and viscoelastic effects prior to rupture whereas after penetration the primary effects are those due to viscous drag of the surrounding material as it is forced against the needle body. The switch from one behaviour to another is simulated using a suitable mathematical function, normally the Heaviside function, $H(x)$. This makes it possible to switch 'on and off' individual tissue types as well as their pre- and post-rupture components, and so build a complete profile. The scheme by which the experimental data and mathematical models are used to form simulation profiles is shown schematically in Fig. 6.

To illustrate the manner in which the mathematical models are used to form a complete force–displacement profile for simulation within the scheme outlined above, the force transients in Fig. 7 should be considered. This stage is marked 'experimental data' in Fig. 6 and forms the start of the processing. This was taken previously from a fixed cadaver using a constant velocity device driving a Tuohy needle. The two prominent peaks correspond to the passage through the skin and the ligamentum flavum while between the two there is a region of slowly increasing frictional force on the needle. The approximation of the individual tissues using models such as those mentioned above is shown in Fig. 8. This corresponds to the section marked 'individual tissue response' in Fig. 6.

The largely elastic skin layer shows an increasing force behaviour terminating abruptly when it becomes ruptured (Fig. 8a). Following this the only effect it may have is a frictional one due to clamping on the needle shaft
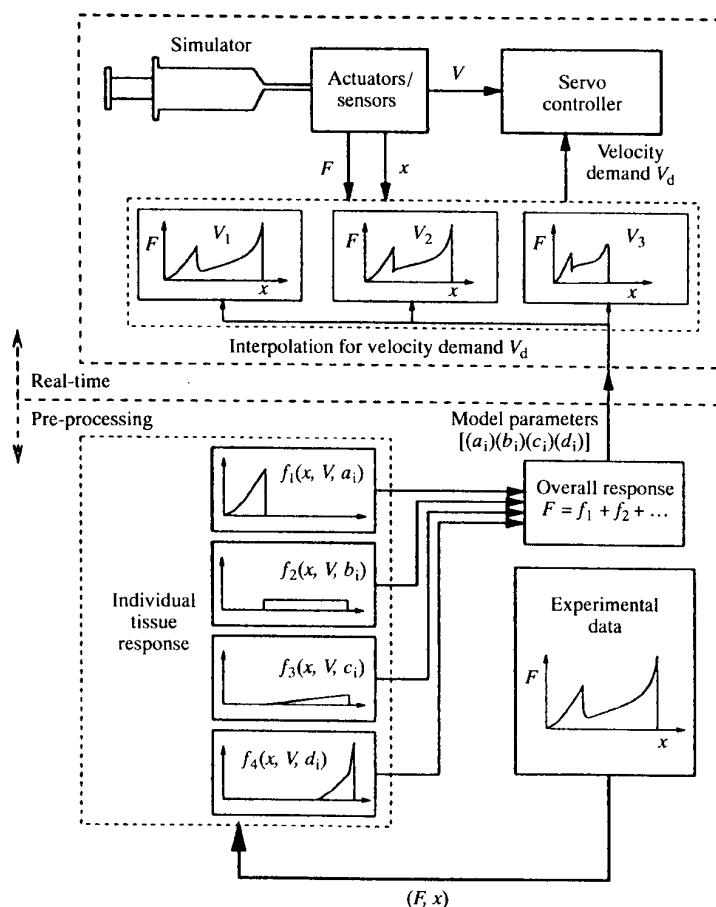
Fig. 6 Schematic representation of the scheme by which experimental data and mathematical models are used to form simulation profiles
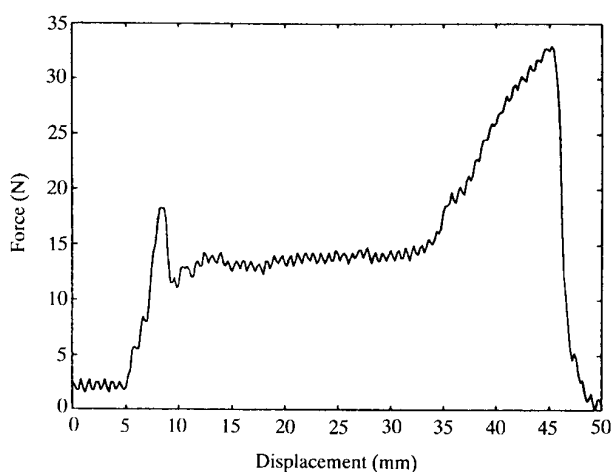

Fig. 7 Force transients

which, as the whole tissue has been penetrated and the skin thickness does not change appreciably, will remain constant at constant needle velocity (Fig. 8b). The subsequent fatty and loose muscle tissue is modelled as a viscous fluid. The magnitude of the resistive force of the fluid at constant velocity is approximately proportional to the surface area of the needle within it. This effect is activated following rupture of the skin and is shown in Fig. 8c. At larger displacements the ligamentum flavum begins to have an effect, showing increasing resistance until its rupture (Fig. 8d).

Addition of these components then leads to a first approximation to the actual force profile as a function of needle displacement, as shown in Fig. 9. The coefficient values obtained by fitting the modelled needle response to each individual tissue layer are then stored, and the process repeated for subsequent experimental profiles. The library of coefficient values are then used in a 'look-up table' manner by the simulator, given the displacement and measured force data from the users input, as described at the end of the section.

There are many existing models of tissue response suitable under various testing regimes, some of which are based on the underlying material properties and some of which are based on empirical studies. To meet the needs of this study the primary interest is a convenient representation of the experimental data to determine the instantaneous velocity response guided by the user
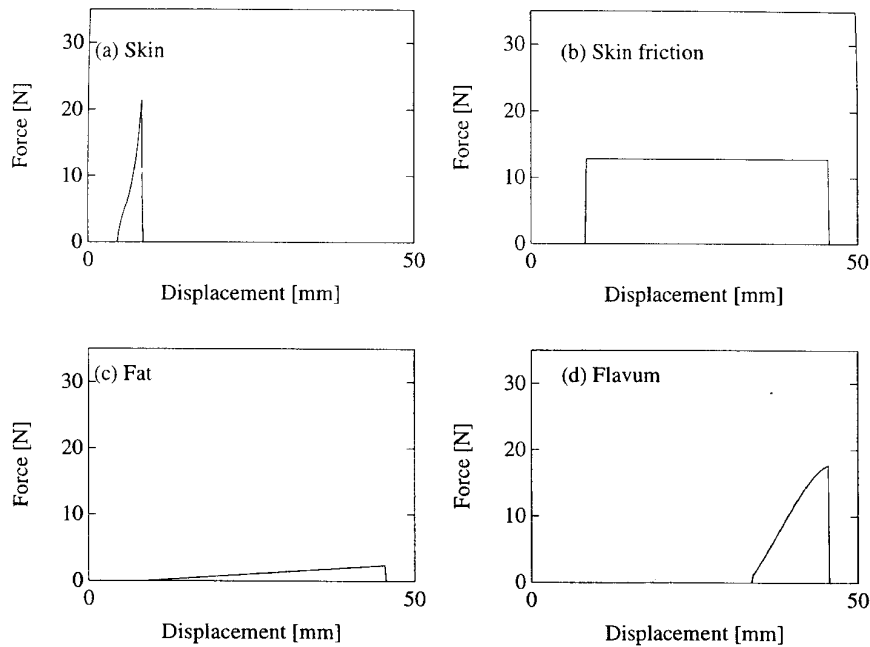
Fig. 8 Force behaviour of skin layer, fatty/loose muscle tissue and ligamentum flavum
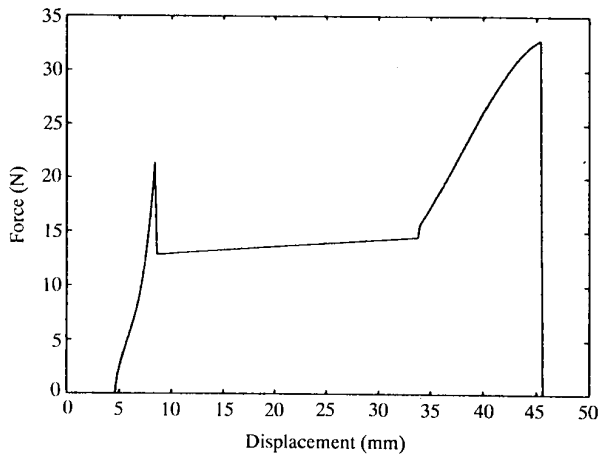

Fig. 9 Approximation to the actual force profile as a function of needle displacement

applied force and needle position as input demand to the simulator. Further, the variation in behaviour of a particular tissue between patients, and also due to physiological and environmental conditions of an individual, may often be greater than the variation between tissue types. This has led to the search for relatively simple describing equations for experimental force data rather than complex and computationally more demanding models derived from detailed tissue component behaviour. To do this, broadly, it was decided to use models that described simple and representative behaviour to separate the soft tissues into three categories according to their dominant behaviour, namely skin, muscular and ligamental tissue (non-linear viscoelastic

solid), connective tissue and fascia (elastic membrane), and fat (viscous solid). The model equations used for each type are described below.

The model used for simulation of needle response in skin and ligamental tissue is based on a finite series of Voigt elements in which the number of elements in the series is increased with displacement. It was assumed that one element was added for each displacement beyond a multiple of a chosen, characteristic length Δx and that there is a linear increase in the elastic modulus of the individual Voigt elements with number of elements. This leads to a relationship between force F and deflection z of the form given in equation (1). The derivation of this relationship is described in Appendix 3

$$F(x) \propto \frac{x(6\eta V \Delta x \times kx^2 + 3kx\Delta x + 2k\Delta x^2)}{6\Delta x^2} \qquad (1)$$

Here η, k are the viscous and elastic constants from the initial Voigt element corresponding to a deflection $x < \Delta x$.

With consideration of the geometric form of the connective tissue and fascia and their physical composition, a model was developed based on the assumption that the tissue could be considered to act as a thin, elastic membrane. It was also assumed that the change in the strain energy of the membrane due to its deformation was proportional to the change in its surface area, and that therefore the final shape of the deformed tissue would be such that its surface area was a minimum. This leads to a relationship between the force F and deflection x at the point of loading given by equation (2).

$$F(x) = 2\pi R_a k \left\{ (x - b) - a \ln \left[\cosh \left(\frac{x - b}{a} \right) \right] \right\} \qquad (2)$$

where R_a is the radius of the needle, k is the elastic modulus and a, b are constants related to the geometry of the tissue and needle.

The mechanical properties of adipose tissue are relatively simple, especially when using a point-like penetrating instrument, as with the hypodermic needles used in the epidural procedure. The tissue is comparatively structureless and may be considered as a homogeneous, isotropic fluid. The fat cells contribute little in the way of material strength from their cell walls which are easily ruptured or parted, leaving the viscous drag from the fat itself on the needle shaft as the dominant effect. The model used for this tissue is a Newtonian viscous fluid where the stress per unit length is proportional to the strain rate. The constant of proportionality is the dynamic viscosity η. For sliding contact between the needle and the fatty tissue, the strain rate of the fluid is equal to the velocity of the needle. The length on which the fat acts is equal to the penetration by the needle until the point at which the needle tip exits the fat. After this the length is given by the depth of the fatty tissue. For a needle of external radius r the total area A on which the resistive force acts at a penetration x through the fat layer of thickness d is then given by equation (3)

$$A(x) = \begin{cases} \pi r x & x \leqslant d \\ \pi d & x > d \end{cases} \tag{3}$$

For a constant velocity this will lead to a linear increase in force $f(x)$ with displacement x given by equation (4)

$$f(x) = \eta V A(x) \tag{4}$$

For high viscosity and small tissue thickness, equation (4) can also be interpreted as an approximately constant force on the needle, as is found, for example, by the action of the skin following rupture.

The initial values for tissue parameters entered into all models were obtained from the existing literature (**17**, **18**) and compared with experimental data, with further tuning being made to correlate model parameters with the standard form of published properties.

The velocity dependence of the peak forces has been estimated from porcine data and is used to scale the simulator response. Modelling of the dependence has been based on average values of least-squares fit from three samples of porcine spinal regions between three and seven hours post mortem and one human post mortem epidural within 24 hours of death.

Interfacial ruptures have been represented by Heaviside functions $H(x_{max} - x)$, where x_{max} is the displacement at which rupture occurs. This has been observed to be a realistic assumption based on mechanically driven, constant velocity experiments on porcine samples. Experimental data from trials where needle progress has been under the control of a human operator have tended to mask the true tissue response upon rupture, due to the nature of the force sensing and the operator's own reactions. Delayed elastic recovery of the ruptured tissue have not been significant in mechanically driven trials.

Following the breakthrough of the needle through the elastic structures, the force data show a distinct frictional component. Data collected to date have indicated that a high percentage of this force is due to large clamping forces on the needle, primarily from the skin, and not from the intrinsic viscosity of the surrounding tissue. This has been demonstrated for porcine samples with intact and excised skin, and to a lesser extent with human cadaveric trials.

The approach to the computational scheme as applied to the simulator is then as follows. First the positions of the tissue types are described, as this enables pre-processing of the model descriptions of force for a set of velocities by summing values for equations (1), (2) and (4) for the full trajectory of the needle. On pushing the needle, the operator applies a force and this value, together with the position measurement of the needle, defines the demand velocity for the simulator. This will need to be computed by interpolation between the modelled needle force transients.

6 DISCUSSION

The force experienced depends upon needle velocity and therefore a variable velocity will produce quite a different force characteristic compared with a steady velocity, although the principal peaks are always present. Typical force measurements from a simulator trial are plotted as a function of displacement in Fig. 7. The plot shows the principal peaks corresponding with initial penetration of skin and fat tissue followed by the intra-spinous ligament and finally the ligamentum flavum. In this instance, before entering the ligamentum flavum, the user dwelled while adjusting grip, resulting in a reduction in force, coincident with the reduced needle velocity. While the simulator is being used the computer stores the force applied with respect to time, and the corresponding velocity of the needle. This information can be displayed and can be used to compare performance with that of an expert. Simulated needle overshoot provides a measure of control over the critical puncture of the ligamentum flavum.

The view of anaesthetists who have used the simulator is that it provides a representative sensation of an epidural puncture. Further investigations are necessary, however, to verify performance and differences in sensation experienced relating to patient types and different techniques for holding the needle and syringe. Characteristics vary between patients of different age, build and fitness and the relationships between these need to be quantified. The method can be developed further. Additional sensations will be experienced on pursuing needle trajectories that may be used in error or

result in contact with bone. Using the same approach, these can be modelled based on measurements.

There is a need to consider a more versatile mechanism; the current device is confined to uniaxial tool action and there would be additional benefit in extending the method to allow a pivoting action about a fulcrum at the surface point on the trajectory, with the action to simulate needle side forces. Measurement of forces will rely on further tests using porcine samples and is the subject of a current research study.

7 CONCLUSIONS

The design of a surgical needle resistance force simulation system has been described that provides a consistent training medium to develop or improve skills required for the epidural procedure. Potentially the system can be used to simulate different patient conditions and procedures, and can provide a measure of the performance of the user. The simulations are based on measured applied force and resulting velocity transients using porcine samples and cadavers. These have shown that similar results are obtained in human and porcine tissue with the exception of penetrating skin and superficial tissues. The principal tissue resistance features to be represented by the simulator are those of puncturing, skin, superficial tissues and ligamenta, and the effect of clamping of the needle by punctured tissue layers.

Mathematical descriptions of needle applied force and corresponding velocity response are represented by a family of curves representing force corresponding with needle velocity and depth of penetration. The velocity demand of the needle is then interpolated from these functions that provided the relationship between measured applied force and needle depth.

The simulator can be used to represent the sensation of administering an epidural on patients of different build and state given that previously measured samples have been obtained. Anaesthetists who have used the simulator have so far indicated that the sensation produced is representative of the experience when administering an epidural. However, a more extensive and controlled study by users will indicate the range of patient morphology that can be represented satisfactorily.

ACKNOWLEDGEMENTS

REFERENCES

1 **Taylor, R. H., Paul, H. A., Mittelstadt, B. D., Hanson, W., Kazankides, P., Zuhars, J. F., Glassman, E., Musits, B. L.,** **Bargar, W. L.** and **Williamson, W.** An image based robotics system for hip replacement surgery. *J. Robotics Soc. of Japan*, October 1990, 111–116.

2 **Drake, J. M., Joy, M., Goldenburg, A.** and **Kreindler, D.** Computer and robotic assisted resection of brain tumours. ICAR 5th International Conference on *Advanced Robotics*; *Robotics in Unstructured Environments*, Pisa, Italy, 19–22 June 1991.

3 **Brett, P. N., Baker, D., Reyes, L.** and **Blanshard J.** An automatic technique for micro-drilling a stapedotomy in the flexible stapes footplate. *Proc. Instn Mech. Engrs, Part H*, 1995, **209**(H4), 255–262.

4 **Potamianos, P., Davies, B. L.** and **Hibberd, R. D.** Intra-operative registration for percutaneous surgery. Proceedings of 2nd International Symposium on *Medical Robotics and Computer Assisted Surgery*, Baltimore, November 1995, pp. 156–164.

5 **Bauer, A., Soldner, E. H., Ziegler, R.** and **Muller, W.** Virtual reality in the surgical arthroscopical training. Proceedings of 2nd International Symposium on *Medical Robotics and Computer Assisted Surgery*, Baltimore, November 1995, pp. 350–354.

6 **Poston, T., Serra, L., Lawton, W.** and **Choon Chun, B.** Interactive tube finding on a virtual workbench. Proceedings of 2nd International Symposium on *Medical Robotics and Computer Assisted Surgery*, Baltimore, November 1995, pp. 119–123.

7 **Runciman, W. B.** Monitoring and patient safety: an overview. *Anaesthesia and Intensive care*, *Austr. J. Anaesthetists*, February 1988, **16**(1).

8 **Fowler, C. G.** Training aids for minimal access therapy. IMechE Seminar on *Minimal Invasive Surgery*, London, 28 Febuary 1995.

9 **Smith, G.** Palpable progress. Article on science and technology in *Business Week*, 9 October 1995, pp. 93–94.

10 **Muller, H. G.** *An Introduction to Food Rheology*, 1973 (Heinnemann, London).

11 **Moss-Salentijn, L.** The human tactile system. In *Advanced Tactile Sensing for Robotics* (Ed. H. R. Nicholls), 1992. Ch. 8, pp. 123–150, Vol. 5 of *Robotics and Automated Systems* (World Scientific).

12 **Brooks, T. L.** Telerobotics response requirements. IEEE International Conference on *Systems, Man and Cybernetics*, 1990, pp. 113–120.

13 **Brett, P. N., Griffiths, M. V., Kamel, Y., Fraser, C.** and **Hennigan, M.** Automatic techniques for controlling the penetration of tools through soft tissues. *IEEE, Engng in Medicine and Biol.*, May 1995, **14**(3), 264–270.

14 **Holloway, T. E.** and **Telford, R. J.** Observations on deliberate dural puncture with a Tuohy needle: depth measurements. *Anæsthesia*, 1991, **46**, 722–724.

15 **Duck, F. A.** *Physical Properties of Tissue*, 1990, pp. 150–162 (Academic Press).

16 **Yamada, H.** *Strength of Biological Materials*, 1970 (Kreiger).

17 **Findley, W. N.** *Creep and Relaxation of Non-linear Viscoelastic Materials: with an Introduction to Linear Viscoelasticity,* Vol. 18, Series in Applied Mathematics and Mechanics, 1976 (North Holland, Amsterdam).

18 **Fung, Y. C.** *Biomechanics*, 1993, Ch. 7, p. 568 (Springer-Verlag).

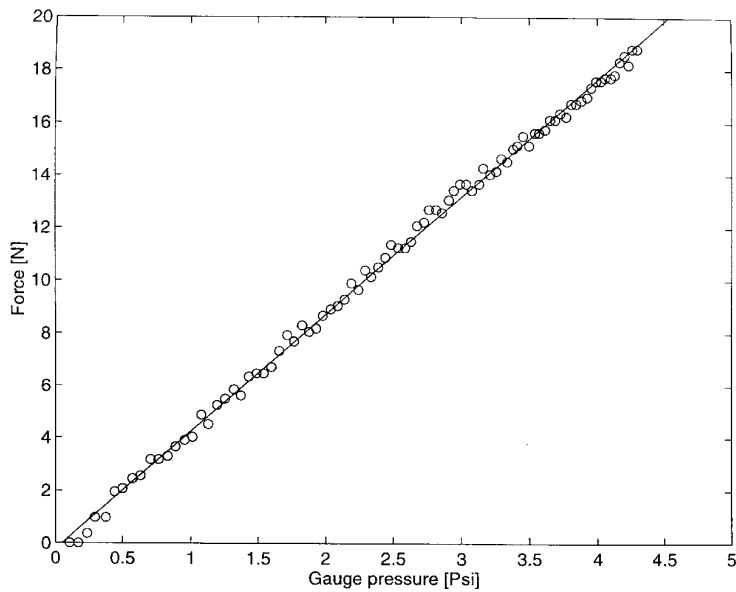## APPENDIX 1

Pressure–force calibration curves

Fig. 10   Pressure–force calibration curves

APPENDIX 2

Proximity sensor calibration curves
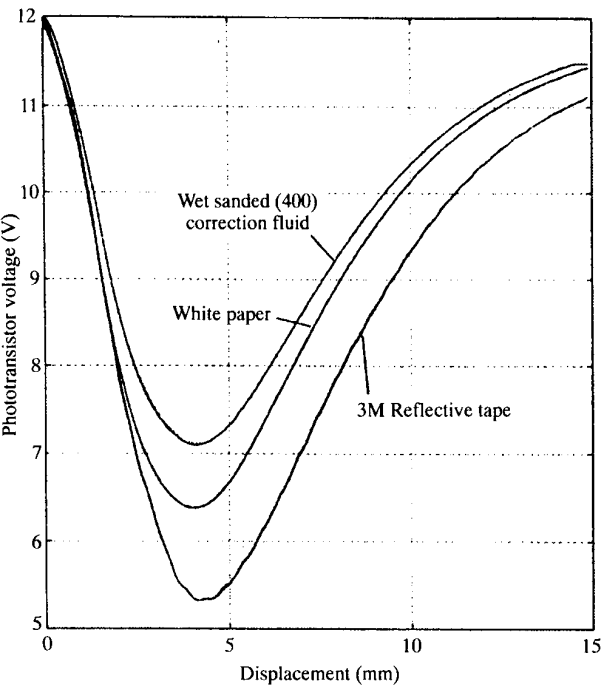

Fig. 11   Proximity sensor calibration curves

APPENDIX 3

An incremental, viscoelastic model of tissue

This model is based on a series of simple viscoelastic units, individually known as a Voigt model (**17**). One such element is shown in Fig. 12 and consists of a purely elastic spring with Young's modulus k, in parallel with
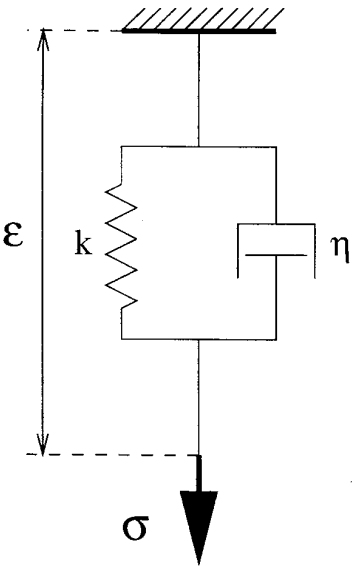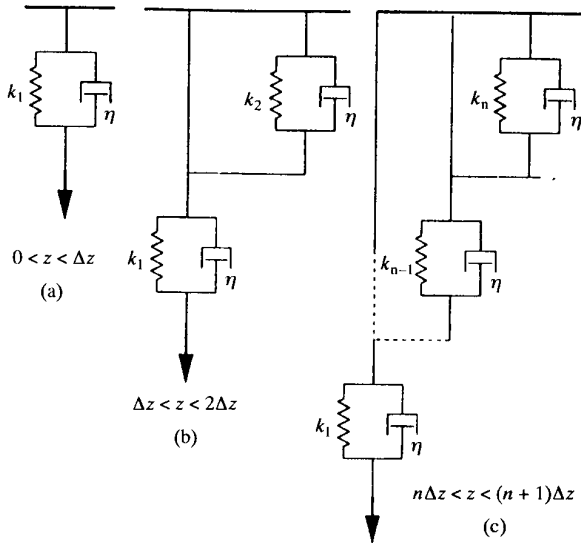

Fig. 12

Fig. 13 Schematic diagram showing the application of additional Voigt elements corresponding with needle displacement

a purely viscous damper of viscosity η. Any strain, ε, induced by a stress, σ, on a material modelled by this element is common in both the spring and the damper.

The stress and strain are related to equation (5)

$$\sigma(t) = k\varepsilon(t) + \eta \frac{d}{dt}\varepsilon(t) \qquad (5)$$

In the following the model will be discussed in terms of force F on the tissue and deflection x of the tissue with the understanding that the geometrical details will be applied in any numerical calculations. For a constant needle velocity V with the tissue not yet ruptured or cut, ε can be related to V and x simply by $\varepsilon = x$, $\varepsilon' = V$. With this, an analogous equation to equation (5) can be written in terms of F and x as

$$F(x) \propto kx + \eta V \qquad (6)$$

Equation (6) is then taken as the governing equation for one Voigt element in a series of similar elements, according to the scheme shown diagrammatically in Fig. 13 and detailed below.

1. A fundamental distance Δx is chosen which will later be related to tissue response, but initially can be some small, arbitrary number that effectively sets the length scale by which the tissue can be analysed.

2. The tissue deformation is increased. If the total deflection x is less than Δx, the tissue behaviour is that given by equation (6) and the corresponding model is shown in Fig. 13. As x increases to Δx a second Voigt element is added which initially has no deflection, i.e. x is replaced in equation (6) by $x - \Delta x$. The total force required to maintain this velocity is then the sum of the forces given by each element.

3. The deformation is increased again. The situation is then similar to Fig. 13b. The suffix on each of the elastic moduli is there to indicate that these may differ from one element to another.

4. The deformation continues to be increased, adding one more element each time x reaches a multiple of Δx, each with a 'reduced' displacement. For the nth element this will be $x - (n-1)\Delta x$. The new force required to maintain the constant velocity is then the sum of the n elements in the model. This is shown schematically in Fig. 13c.

This process ends in practice when the displacement is equal to the final displacement of the trial or until the tissue ruptures. After N increments, the force experienced is then given by equation (7).

$$F(z, N) \propto \sum_{n=1}^{N} k[x - (n-1)\Delta x] + \eta V \qquad (7)$$

where n is the summation variable. N is dependent on Δx and is equal to x div Δx, i.e. the integer quotient of $x/\Delta x$. Performing the summation, the following is obtained:

$$F(x) \propto \frac{x(kx + k\Delta x + 2\eta V)}{2\Delta x} \qquad (8)$$

Variations can be made to the spring and damper constants, k and η to account for different tissue effects. One such variation that was tried was to start with k equal to some initial value, say k_0 and then increase k in subsequent elements. One of the simplest variations for k is a linear increase with n such as equation (9)

$$k \to nk_0 \qquad (9)$$

Substituting this into equation (7) and performing the summation, the relationship between F and z given in the text is obtained, namely

$$F(z) = \frac{z(6\eta V\Delta z + k_0 z^2 + 3k_0 z\Delta z + 2k_0 \Delta z^2)}{6\Delta z^2} \qquad (10)$$